Mixed-Integer Optimal Control for Multimodal Chromatography

Hans Georg Bock[a], Dominik H. Cebulla[b,*], Christian Kirches[b], Andreas Potschka[a]

[a] *Interdisciplinary Center for Scientific Computing (IWR), Heidelberg University, 69120 Heidelberg, Germany*
[b] *Institute for Mathematical Optimization, Technische Universität Carolo-Wilhelmina zu Braunschweig, 38106 Braunschweig, Germany*

Abstract

Multimodal chromatography is a powerful tool in the downstream processing of biopharmaceuticals. To fully benefit from this technology, an efficient process strategy must be determined beforehand. To facilitate this task, we employ a recent mechanistic model for multimodal chromatography, which takes salt concentration and pH into account, and we present a mathematical framework for the optimization of chromatographic processes. This framework also includes the use of discrete process controls in order to cover a wider range of chromatographic applications. We describe a procedure to numerically solve the resulting nonlinear mixed-integer optimal control problems. We discuss results of computational experiments, covering the cases where one wants to optimize the yield of the product or the batch-cycle time under specified purity requirements. The results indicate that a good separation can be achieved in a two-component system and that both salt concentration and discrete pH play an important role within the purification process.

Keywords: Multimodal chromatography, Nonlinear mixed-integer partial differential equation constrained optimization, Optimal control, Partial outer convexification
2010 MSC: 34H05, 35Q93, 49M20, 90C11, 92C40

1. Introduction

Chromatography is the method of choice in the downstream processing of biopharmaceuticals, being "the only separation process that can deliver a high

*Corresponding author
Email addresses: bock@iwr.uni-heidelberg.de (Hans Georg Bock), d.cebulla@tu-bs.de [ORCID 0000-0002-3025-8673] (Dominik H. Cebulla), c.kirches@tu-bs.de [ORCID 0000-0002-3441-8822] (Christian Kirches), potschka@iwr.uni-heidelberg.de [ORCID 0000-0002-6027-616X] (Andreas Potschka)

purity product" (Mollerup, 2006). Major developments have been achieved in the field of chromatography in recent years—both in academia and industry, cf. Staby et al. (2017)—and development is still going on, for example in the improvement of chromatographic resins, in the creation of alternative chromatography formats, but also in the growing process understanding (Rathore et al., 2018). The latter is also encouraged by the U.S. Food and Drug Administration (FDA), where a deeper insight into the process is thought to improve the pharmaceutical development, manufacturing, and quality assurance (U.S. Food and Drug Administration, 2004).

One possibility to enhance process understanding is the development and use of mechanistic models. One of the major advantages of such models is that they can support the process optimization, given that they are carefully calibrated and describe the underlying process sufficiently well. Hence expensive and time-consuming trial and error experiments can be avoided.

In this paper we focus on column liquid chromatography processes, where a liquid solvent is pumped through a column that is packed with adsorbent particles. Multiple (semi-) mechanistic models for this type of chromatography already exist and we refer to the books of Guiochon et al. (2006) and Schmidt-Traub et al. (2012) for further information.

However, care must be taken when modeling the actual adsorption process. On the one hand, separation of a mixture can be achieved by exploiting several component-specific properties such as electrostatic properties (ion-exchange chromatography), hydrophobic properties (hydrophobic interaction chromatography), or a combination of these (multimodal chromatography). For a detailed description of these techniques, including applications, we refer to Janson (2011) and Kallberg et al. (2012) and the references cited therein. On the other hand, the actual adsorption behavior can be influenced in a complex manner by quantities such as pH, salt (concentration), solvents, flow rate, and temperature (Mollerup, 2006). Given a specific application, one has to identify the quantities that must be taken into account and the actual model should reflect this decision. A literature overview of modeling approaches that deal with the incorporation of some of the aforementioned quantities is given by Leweke and von Lieres (2018).

In the last two decades, multimodal chromatography (MMC) emerged as a powerful and versatile tool in the downstream processing of biopharmaceuticals, see e.g. Zhao et al. (2009), Kallberg et al. (2012), and Zhang and Liu (2016). As mentioned earlier, MMC exerts interactions based on *multiple* physicochemical properties. Therefore, a high selectivity is achievable with this type of chromatography, potentially reducing the number of chromatography steps within the downstream process. The latter is of particular interest, as chromatography steps make up to 70% of the total costs in the downstream processing of biopharmaceuticals (Osberghaus et al., 2012a). The economic gain can hence be considerable.

However, due to its multiple interactions, MMC is a prime example of a chromatography method that is influenced by e.g. salt concentration, pH, and (further) mobile phase modulators in a complex way, compare Wolfe et al. (2014)

and Zhu and Carta (2016). Consequently, it is a challenging task to set up a mechanistic model as well as an optimal process strategy for MMC.

1.1. Contribution

In liquid chromatography so-called bind-and-elute experiments are often performed, meaning that the process conditions are chosen in such a way that the desired product is adsorbed and that (ideally all) impurities simply pass through the column. Afterwards, the process conditions are altered, for example by changing the buffer composition, in order to remove the product from the ligand. In our case, changing the buffer composition is performed by adjusting the buffer salt concentration or the pH (or both). Changing the buffer salt concentration is usually done in a step-wise (step gradient) or in a linear manner (linear gradient), the latter possibly having a "kink" (bilinear salt gradient). Depending on the actual application, the pH is determined by predefined buffer solutions and can not be changed continuously, but one can only choose between finitely many buffer solutions.

Although (real-time) optimization of continuously operated chromatography processes such as Simulated Moving Bed (SMB) or Multi-Column Solvent Gradient Purification (MCSGP) processes has already been reported (see e.g. Potschka, 2014; Behrens et al., 2014), the numerical optimization of a chromatography process, is—to the best of our knowledge—usually performed by a prior decision whether to use a step, linear, or bilinear (salt) gradient that are defined by e.g. their slope and duration (Karlsson et al., 2004; Osberghaus et al., 2012b; Huuk et al., 2014; Leweke and von Lieres, 2018). This approach is somewhat limiting, since it might be more beneficial to perform gradients with multiple kinks and with e.g. positive and negative slopes. Furthermore, the pH is mostly kept fixed or varies only continuously over a small range.

With these preliminary remarks, we summarize our contributions as follows: We present a mathematical framework for optimal control problems (OCPs) for (batch) column liquid chromatography where the process controls are defined on a continuous time domain, thus enhancing our scope for optimization. Particularly, we are not limited to perform a single linear gradient, but the gradients can have multiple kinks and can also have positive and negative slopes. We furthermore generalize our problem formulation by providing the possibility to use discrete-valued process controls. Moreover, we recommend to use a recently introduced binary control to the OCP formulation that signifies whether the eluate is collected or not (Cebulla et al., 2020). In our opinion, introducing this "collect" control is a more flexible and intuitive approach than the determination of a *single* collection interval. For example, being able to turn the eluate collection off and on multiple times is certainly useful if one is interested in collecting more than one component. In order to demonstrate the capabilities of our framework, we apply it to an MMC application by using a slightly modified version of a highly nonlinear adsorption model that has been described previously (Cebulla et al., 2019).

1.2. Outline

This paper is organized as follows: First we present a mechanistic model for column liquid chromatography with an emphasis on a recent adsorption kinetics for MMC. Afterwards, we present concrete instances of OCPs for MMC where the pH and the collect control are modeled as discrete process controls. We then describe a numerical solution procedure for the resulting mixed-integer optimal control problems (MIOCPs) constrained by partial differential equations (PDEs). This includes the description of a high-order finite volume scheme for the spatial discretization of our PDE model, a partial outer convexification and relaxation approach to transform the MIOCPs into continuous ones, and, eventually, a single shooting approach to transform the continuous OCPs into nonlinear programming (NLP) problems. A discussion of results based on computational experiments is presented subsequently. We conclude with a short outlook on possible extensions to our framework.

2. Mechanistic Model for MMC

In column liquid chromatography, a liquid solvent (mobile phase) is pumped through a column that is packed with adsorbent particles (stationary phase). Components—in our case usually proteins—of a mixture are separated by exploiting their different adsorption behaviors. As described earlier, the latter can be influenced e.g. by shifting the pH or changing the buffer salt concentration.

We divide the presentation of the mechanistic model into two parts: First, we present a column model that describes the flow of the mobile phase through the column, as well as the transition into the particle (stationary) phase. This leads to a system of PDEs, which will be completed with suitable initial and boundary conditions. The second part presents a kinetic formulation for the actual MMC adsorption process within the stationary place.

2.1. Column Model

To describe the column liquid chromatography process, we use a transport-dispersive model with adsorption kinetics, sometimes called a "lumped pore model" (Guiochon, 2002). It takes several effects into account, such as convective transport, axial dispersion—which combines multiple diffusive effects, such as Eddy diffusion and the influence of packing tortuosity—and mass transfer between the mobile and the stationary phase. The model is based on the following assumptions: The stationary phase is homogeneous and packed with spherical particles having a constant diameter, fluid density and viscosity are constant, the process is isothermal, the column is radially homogeneous, and there is no convective flow inside the particles. A more detailed description of the underlying model assumptions, as well as further models for column liquid chromatography, can be found in the books of Guiochon et al. (2006) and Schmidt-Traub et al. (2012).

The lumped pore model describes the concentration profiles of all components $i \in \{1, \dots, n_{\text{comp}}\}$ along the axial position $x \in [0, L]$ of the column for a given time $t \in [0, T]$. The model is given by the PDE system

$$\begin{aligned}
\frac{\partial c_i}{\partial t}(t,x) = &- \frac{v_{\text{sup}}}{\varepsilon_b}\frac{\partial c_i}{\partial x}(t,x) + D_{\text{ax}}\frac{\partial^2 c_i}{\partial x^2}(t,x) \\
&- \frac{1-\varepsilon_b}{\varepsilon_b}\frac{3}{r_p}k_{\text{eff},i}\left(c_i(t,x) - c_{p,i}(t,x)\right), \\
\frac{\partial c_{p,i}}{\partial t}(t,x) = &- \frac{(1-\varepsilon_p)}{\varepsilon_p}\frac{\partial q_i}{\partial t}(t,x) + \frac{3}{\varepsilon_p r_p}k_{\text{eff},i}\left(c_i(t,x) - c_{p,i}(t,x)\right).
\end{aligned} \tag{1}$$

The states in this model are the concentrations of the mobile phase c_i, the liquid particle (stationary) phase $c_{p,i}$, and the adsorbed particle phase q_i. The first equation in (1) is a PDE model describing the transport of a component within the column, as well as the mass transfer between mobile phase and liquid particle phase. This equation can be interpreted as an instationary convection-diffusion-reaction equation with a source/sink term. The second equation in (1) is a spatially distributed ordinary differential equation (ODE) that describes the adsorption process in the stationary phase and the transition into the mobile phase. The actual adsorption kinetics, in our case describing the MMC adsorption behavior, is represented by $\partial q_i/\partial t$ and described later.

The model parameters occurring in (1) are the bed porosity ε_b (also known as void fraction), the particle porosity ε_p, an axial dispersion coefficient D_{ax}, a component dependent effective mass transfer coefficient $k_{\text{eff},i}$ that lumps together the actual film mass transfer and the diffusion within the particle pores, and the particle radius r_p. The superficial flow velocity v_{sup} is a process control. Note that the axial dispersion coefficient D_{ax} is sometimes modeled as dependent on the flow velocity (van Deemter et al., 1956; Persson et al., 2006; Schmidt-Traub et al., 2012), but here we consider it as constant.

Before completing the PDE model (1) with initial and boundary conditions, we highlight the occurrence of two additional components representing the buffer solution, namely salt (the modulator, e.g. sodium chloride) and pH. We recently proposed that the latter is modeled as the concentration of protons H^+ in the particle phase (Cebulla et al., 2019),

$$\text{pH} = \text{pH}(t,x) = -\log_{10}(c_{p,\text{H}^+}(t,x)),$$

hence making the pH also dependent on the spatial position and not only on time. The concentration of the salt component is given by the concentration of the actual salt component, e.g. $c_{\text{salt}} = c_{\text{NaCl}}$.

Now we cam complete the PDE model with suitable initial and boundary conditions. Initially, the column does not contain any of the components $i \in \{1, \dots, n_{\text{comp}}\}$, but is equilibrated with a user-defined initial salt concentration

$c_{\text{salt,init}}$ and pH value pH_{init}. Hence the initial conditions read for $x \in (0, L)$,

$$\begin{aligned} &c_i(0,x) = 0, && c_{p,i}(0,x) = 0, && q_i(0,x) = 0, \\ &c_{\text{salt}}(0,x) = c_{\text{salt,init}}, && c_{p,\text{salt}}(0,x) = c_{\text{salt,init}}, && q_{\text{salt}}(0,x) = \Lambda_{\text{IEX}}, \\ &c_{\text{H}^+}(0,x) = 10^{-\text{pH}_{\text{init}}}, && c_{p,\text{H}^+}(0,x) = 10^{-\text{pH}_{\text{init}}}, && q_{\text{H}^+}(0,x) = 0, \end{aligned} \tag{2}$$

where Λ_{IEX} is the ionic capacity of the adsorbent that we will introduce in the description of the MMC adsorption model.

The boundary conditions are due to Danckwerts (1953), with a Robin boundary condition at column inlet and a Neumann (no-flux) boundary condition at column outlet. For $t \in (0, T)$ they are given by

$$\frac{\partial c_i}{\partial x}(t,0) = \frac{v_{\text{sup}}}{\varepsilon_b D_{\text{ax}}} \left(c_i(t,0) - c_{\text{in},i}(t) \right), \quad \frac{\partial c_i}{\partial x}(t,L) = 0. \tag{3}$$

Here, an additional control enters the PDE model, namely $c_{\text{in},i}$, being the inlet concentration for each component $i \in \{1, \ldots, n_{\text{comp}}, \text{salt}, \text{H}^+\}$. Note that if the axial dispersion coefficient D_{ax} is very small, the boundary condition at column inlet is essentially a Dirichlet boundary condition $c_i(t,0) = c_{\text{in},i}(t)$.

This completes the description of the column model and we now draw our attention to the MMC adsorption behavior.

2.2. Adsorption Kinetics for MMC

Since ion-exchange chromatography (IEX) and hydrophobic interaction chromatography (HIC) are the most widely used chromatography types in the downstream processing of biopharmaceuticals, most (if not all) MMC ligands contain functional groups based on these two interactions (Zhao et al., 2009). Note, however, that further interactions such as hydrogen bonding or hydrophilic interactions may occur in MMC. We assume that electrostatic and hydrophobic interactions are the dominating forces. Consequently, our MMC model is based on existing models for IEX and HIC.

IEX and HIC are complementary chromatography methods in the following sense, compare Nfor et al. (2010): Roughly speaking, one uses low salt concentrations in IEX to bind substances and high salt concentrations for elution, whereas the opposite is true for HIC. Furthermore, if the pH is close to the isoelectric of a protein, then hydrophobic interactions will typically dominate; moving away from the isoelectric point by changing the pH will strengthen the electrostatic interactions. Based on these considerations, one can already expect a complex elution behavior when combining IEX and HIC. Moreover, it becomes clear that salt and pH are crucial process controls.

Models for IEX that consider the salt concentration are e.g. the steric mass action (SMA) formalism developed by Brooks and Cramer (1992), where the salt component is an intrinsic part of the model, or a Langmuir-type isotherm with a mobile phase modulator (MPM), see e.g. Karlsson et al. (2004). The pH dependence can be incorporated in multiple fashions, see e.g. Mollerup (2008), Nfor et al. (2010), and Benner et al. (2019).

Although the main driving forces in HIC do not seem to be as well understood as in IEX, see e.g. the discussion given by Mollerup (2006), models for HIC were developed by e.g. Mollerup (2006), Deitcher et al. (2010), and Wang et al. (2016), although the effects of salt on hydrophobic interactions has been studied much earlier (Melander and Horváth, 1977).

Our MMC isotherm model builds upon the thermodynamic framework developed by Mollerup (2006, 2007, 2008) and is a combination of the HIC isotherm model developed by Deitcher et al. (2010) and the SMA formalism for IEX developed by Brooks and Cramer (1992), with additional modifications to take pH dependency into account. The model is based on the (informal) chemical equilibrium

$$\mathrm{P}_{\mathrm{sol},i} + \nu_i \,(\mathrm{LS}) + n_i \mathrm{L} \rightleftharpoons \mathrm{P}_{\mathrm{ads},i} + \nu_i \mathrm{S} + n_i \xi \mathrm{W}, \tag{4}$$

which states that the ith solute protein $\mathrm{P}_{\mathrm{sol},i}$ interacts simultaneously with ν_i adsorbed salt ions LS and n_i hydrophobic ligands L. Thus, the protein gets adsorbed ($\mathrm{P}_{\mathrm{ads},i}$), ν_i salt ions S are released from the stationary phase and ξ water molecules W are displaced from the protein and ligand for every protein–ligand contact. For simplicity, we assume that the salt ions and the charged groups on the ligand are monovalent.

The equilibrium constant for (4) is given in terms of activities by

$$K_i = \left(\frac{a_{\mathrm{P}_{\mathrm{ads},i}}}{a_{\mathrm{P}_{\mathrm{sol},i}}} \right) \left(\frac{a_{\mathrm{S}}}{a_{\mathrm{LS}}} \right)^{\nu_i} \left(\frac{1}{a_{\mathrm{L}}} \right)^{n_i} a_{\mathrm{W}}^{\xi n_i} \tag{5}$$

and the idea is to parameterize all activities in this equation by concentrations and activity coefficients. Following the derivations by Cebulla et al. (2019), we arrive at the modified equilibrium constant

$$\widetilde{K}_i = \frac{q_i}{\widetilde{\gamma}_{\mathrm{sol},i} c_{p,i}} \left(\frac{c_{p,\mathrm{salt}}}{\hat{q}_{\mathrm{salt}}} \right)^{\nu_i} \left(\frac{\tilde{c}}{\hat{c}_{\mathrm{L}}} \right)^{n_i} \exp\left(\rho \, \xi \, n_i \, c_{p,\mathrm{salt}} \right). \tag{6}$$

Note that in the following, we omit the argument (t, x) for the PDE states in favor of an uncluttered presentation. We briefly give an interpretation of the quantities occurring in (6).

The asymmetric activity coefficient of the ith protein in solute phase is parameterized by Nfor et al. (2010) as

$$\widetilde{\gamma}_{\mathrm{sol},i} = \exp\left(\kappa_{\mathrm{salt},i} \, c_{p,\mathrm{salt}} + \kappa_{\mathrm{P},i} \, c_{p,i} \right) \approx \exp\left(\kappa_{\mathrm{salt},i} \, c_{p,\mathrm{salt}} \right), \tag{7}$$

with parameters $\kappa_{\mathrm{salt},i}$ and $\kappa_{\mathrm{P},i}$ indicating which of protein–water, protein–salt and protein–protein interaction is the dominating one. The last approximation often holds since the concentration of proteins in the particle phase $c_{p,i}$ is generally several orders of magnitude smaller than the salt concentration in the particle phase $c_{p,\mathrm{salt}}$. Note that Deitcher et al. (2010) also introduce an asymmetric activity coefficient for the ith protein in the *adsorbed* phase to account for lateral interactions between adsorbed proteins. However, we assume the activity coefficient to be constant, as is also done by Mollerup (2007) and Nfor et al. (2010).

The quantity $\hat{q}_{\text{salt}}$ denotes the concentration of adsorbed salt ions available for protein binding. Based on the SMA formalism (Brooks and Cramer, 1992), it is given by

$$\hat{q}_{\text{salt}} = \Lambda_{\text{IEX}} - \sum_{j=1}^{n_{\text{comp}}} (\nu_j + \varsigma_j)\, q_j, \tag{8}$$

where Λ_{IEX} is the ionic capacity of the charged groups on the stationary phase, ς_i accounts for adsorbed, but blocked salt ions due to the size of the proteins, and ν_i denotes the binding charge of the ith component as introduced in (4).

Analogously, the concentration of available ligands for hydrophobic interactions is given by

$$\hat{c}_{\text{L}} = \Lambda_{\text{HIC}} - \sum_{j=1}^{n_{\text{comp}}} (n_j + \delta_j)\, q_j, \tag{9}$$

where Λ_{HIC} is the ligand density of the stationary phase, δ_i is a shielding factor, and n_i denotes the "multiplicity" of hydrophobic ligand binding, compare (4).

Jenkins (1998) observes that for many salts in concentrations of interest, a linear relationship between $\ln a_{\text{W}}$ and the salt concentration holds and the model parameter ρ is the corresponding proportionality factor. Finally, the concentration of the solution (water) $\tilde{c}$ is assumed to be constant (unity).

Inserting (7), (8), and (9) into (6) and transforming the resulting formula into kinetic form, we arrive at the following highly nonlinear MMC adsorption kinetics for $i \in \{1, \ldots, n_{\text{comp}}\}$,

$$\begin{aligned} \frac{\partial q_i}{\partial t} = \Bigg[& k_{\text{eq},i} \left(\Lambda_{\text{IEX}} - \sum_{j=1}^{n_{\text{comp}}} (\nu_j + \varsigma_j)\, q_j \right)^{\nu_i} \left(\Lambda_{\text{HIC}} - \sum_{j=1}^{n_{\text{comp}}} (n_j + \delta_j)\, q_j \right)^{n_i} \\ & \exp\left(\left[\kappa_{\text{salt},i} - \rho\, \xi n_i \right]\, c_{p,\text{salt}} \right) c_{p,i} - \tilde{c}^{n_i} q_i \left(c_{p,\text{salt}} \right)^{\nu_i} \Bigg] k_{\text{kin},i}. \end{aligned} \tag{10}$$

Here $k_{\text{eq},i}$ and $k_{\text{kin},i}$ are further parameters that must be determined, the first resembling the (modified) equilibration constant in (6), the latter signaling how fast the ad- and desorption process takes place.

Note that if $\nu_i \approx 0$, then (10) reduces to a kinetic version of the HIC isotherm proposed by Deitcher et al. (2010). If, on the other hand, $n_i \approx 0$, then (10) is similar to the "generalized" IEX isotherm described by Huuk et al. (2017). Hence this model can reflect both "pure" IEX and HIC behavior.

The pH enters the adsorption kinetics by parameterizing the equilibrium constant and binding charge according to

$$\begin{aligned} k_{\text{eq},i} &= k_{\text{eq},i}(\text{pH}) = k_{\text{eq},0,i} \exp\left(\gamma_{\text{pH},i} \left[\text{pH}(t,x) - \text{pH}_{\text{ref}} \right] \right), \\ \nu_i &= \nu_i(\text{pH}) = \nu_{i,1} \log \text{pH}(t,x) + \nu_{i,2}, \end{aligned} \tag{11}$$

(Mollerup, 2008; Benner et al., 2019). Here, pH_{ref} denotes a user-defined reference value for the pH (typically the equilibration pH), $\gamma_{\text{pH},i}$ is a component dependent weighting factor analogously to a Langmuir MPM model (see e.g.

Karlsson et al., 2004), $\nu_{i,1}$ and $\nu_{i,2}$ are further parameters that have to be determined. Note that by using the above parameterization, $k_{\mathrm{eq},i}$ and ν_i become (implicitly) dependent on time *and* space.

Finally, we have to present the adsorption behavior for the salt and pH component, the latter given by the concentration of protons. We assume that the protons are inert, hence no adsorption takes place. This is in accordance with the chosen initial value for the adsorbed phase of the proton component (2). For the salt component an electroneutrality condition must hold (Brooks and Cramer, 1992): All charged binding sites must be occupied with either salt ions or proteins. This eventually leads to

$$\frac{\partial q_{\mathrm{H}^+}}{\partial t} \equiv 0, \qquad \frac{\partial q_{\mathrm{salt}}}{\partial t} = -\sum_{j=1}^{n_{\mathrm{comp}}} \nu_j \frac{\partial q_j}{\partial t}.$$

Having presented the adsorption behavior for all components, including salt and pH, the description of the kinetic MMC isotherm model is completed.

3. Optimal Control for Column Liquid Chromatography

In this section, we are first going to introduce concrete examples of OCPs for (general) column liquid chromatography processes. To this end, we define several optimization criteria; furthermore, we highlight the incorporation of discrete process controls into our problem formulation. Afterwards, we describe a procedure for the numerical solution of the underlying nonlinear mixed-integer PDE-constrained optimization (MIPDECO) problems. We conclude this section with a note on the regularization of process controls, which is necessary for a unique determination of the optimal control trajectories.

3.1. Optimal Control Problems for Liquid Column Chromatography

One of the main reasons to develop mechanistic models is to optimize the underlying real-world process with respect to certain objectives and constraints. In column liquid chromatography, typical quantities of interest are yield and purity of a product, batch-cycle time, productivity, and others. These quantities can then be used, for example, to quantify the efficiency of chromatographic resins (Nfor et al., 2011) or the efficiency of a specific separation process. We only introduce the quantities we are going to use for our case studies and we refer to e.g. Schmidt-Traub et al. (2012) where further optimization criteria are defined for both batch and continuously operated chromatography processes.

We first define the injected, eluted ("outflowing"), and collected amount of

a substance $i \in \{1, \dots, n_{\text{comp}}\}$ at given time $t \in [0, T]$. These are given by

$$m_{\text{in},i}(t) = \dot{V} \int_0^t c_{\text{in},i}(\tau) \, \mathrm{d}\tau, \tag{12a}$$

$$m_{\text{out},i}(t) = \dot{V} \int_0^t c_i(\tau, L) \, \mathrm{d}\tau, \tag{12b}$$

$$m_{\text{coll},i}(t) = \dot{V} \int_0^t c_i(\tau, L) \, \text{coll}(\tau) \, \mathrm{d}\tau. \tag{12c}$$

Here, $\dot{V}$ is the volumetric flow rate, which can be computed from the superficial flow velocity v_{sup} (and vice versa), and $\text{coll}(t) \in \{0, 1\}$ is a measurable binary-valued control function that indicates whether we are collecting at time t or not (Cebulla et al., 2020). At this point, we highlight that in the literature, see e.g. Nfor et al. (2011), Schmidt-Traub et al. (2012), and Leweke and von Lieres (2018), the collected amount of a substance is usually defined over a specific interval $[t_1, t_2]$, with $0 \leq t_1 < t_2 \leq T$, and one has to find suitable values for the so-called cut points t_1 and t_2. However, we propose to use the more flexible approach by introducing the binary control $\text{coll}(t)$ as we then can turn the corresponding eluate collection off and on multiple times instead of being restricted to a single time interval $[t_1, t_2]$. Of course, this introduces a mixed-integer aspect into our control problem, which must be treated appropriately.

The actual optimization criteria are based upon the above defined amount of substances (12). The yield of a component $i \in \{1, \dots, n_{\text{comp}}\}$ is defined as the fraction of the collected amount of the substance at a given time t over the total injected amount of that substance. Hence,

$$\text{Yield}_i(t) = \frac{m_{\text{coll},i}(t)}{m_{\text{in},i}(t)}.$$

The purity of a component i is defined as the fraction of the collected amount of the component over the collected amount of all components. We thus have

$$\text{Purity}_i(t) = \frac{m_{\text{coll},i}(t)}{\sum_{j=1}^{n_{\text{comp}}} m_{\text{coll},j}(t)}.$$

Of course, these quantities are only defined if the denominator does not equal zero, so at least we necessarily must have $t > 0$.

We now introduce two instances of OCPs for column liquid chromatography processes. To this end, let $* \in \{1, \dots, n_{\text{comp}}\}$ denote the desired component (product).

Informally, the first OCP reads, for a *fixed* batch-cycle time T,

$$\begin{aligned} \max \quad & \text{Yield}_*(T) \\ \text{s.t.} \quad & \text{Purity}_*(T) \geq \text{Purity}_{\text{min},*}, \\ & \frac{m_{\text{out},i}(T)}{m_{\text{in},i}(T)} \geq \zeta_i \in [0, 1], \end{aligned} \tag{13}$$

hence the goal is to maximize the yield of the product subject to a lower bound on its purity. Furthermore, the last inequality ensures that $\zeta_i \cdot 100\%$ amount of substance entering the column has also left the column at the end of the batch cycle (for *every* component $i \in \{1, \ldots, n_{\text{comp}}\}$). Note that we can omit the last inequality if we are, for example, not interested in the state of the column after optimization.

For a *free* batch-cycle time T, the second OCP is given by

$$\begin{aligned} \min \quad & T \\ \text{s.t.} \quad & \text{Purity}_*(T) \geq \text{Purity}_{\text{min},*} \\ & \text{Yield}_*(T) \ \geq \text{Yield}_{\text{min},*}, \\ & \frac{m_{\text{out},i}(T)}{m_{\text{in},i}(T)} \ \geq \zeta_i \in [0,1]\,, \end{aligned} \tag{14}$$

i.e. here we want to minimize the batch-cycle time T, while still ensuring a sufficiently high yield and purity of the product. A "good guess" for the lower bound on the yield can be obtained by solving (13) beforehand.

To complete the OCPs, we have to add constraints for the controls, which must be satisfied for almost all $t \in [0, T]$. In our case, for a user-defined *fixed* feed inlet time $t_{\text{in}} \in (0, T)$, these constraints are given by

$$c_{\text{in},i}(t) \quad = \begin{cases} c_{\text{load},i}, & \text{for } 0 \leq t \leq t_{\text{in}}, \\ 0, & \text{for } t > t_{\text{in}}, \end{cases} \tag{15a}$$

$$c_{\text{in,salt}}(t) \in \left[\underline{c_{\text{in,salt}}}, \overline{c_{\text{in,salt}}}\right], \tag{15b}$$

$$c_{\text{in,salt}}(t) = c_{\text{salt,init}}, \qquad \text{for } 0 \leq t \leq t_{\text{in}}, \tag{15c}$$

$$c_{\text{in,H}^+}(t) \in \{10^{-\text{pH}_1}, \ldots, 10^{-\text{pH}_k}\}, \tag{15d}$$

$$c_{\text{in,H}^+}(t) = 10^{-\text{pH}_{\text{init}}}, \qquad \text{for } 0 \leq t \leq t_{\text{in}}, \tag{15e}$$

$$\text{coll}(t) \quad \in \{0, 1\}. \tag{15f}$$

The first constraint (15a) states that the mixture, given by known feed concentrations $c_{\text{load},i}$ for $i \in \{1, \ldots, n_{\text{comp}}\}$, is fed into the column only during the inlet phase $t \in [0, t_{\text{in}}]$. This is motivated by bind-and-elute experiments, where a certain amount of input is fed into the column (typically under binding conditions for the product) and afterwards the feed inlet is turned off and the process conditions are modified to elute the product from the column. The subsequent constraints are bounds on the salt inlet concentration (15b) and the ranges for the discrete controls (15d), (15f). Finally, we do not allow the buffer composition (salt concentration and pH) to change during the feed inlet phase, (15c), (15e). This is justified if the feed (mixture) and the buffer solution are injected with different pumps that can not operate simultaneously. During feed inlet time, the buffer composition is thus fixed at the equilibration concentration, as given by the initial values of the PDE model (2). If the batch-cycle time T is subject to optimization, we of course must impose bounds on this variable, too (not shown here).

3.2. Numerical Solution Procedure

Both OCPs (13) and (14) belong to the challenging class of MIPDECO problems, as the optimization quantities are dependent on the states of the PDE model (1) and since some of the process controls are discrete-valued. We highlight that this problem class attains much interest in current research (see e.g. Hante and Sager, 2013; Buchheim et al., 2018; Manns and Kirches, 2020). Based on our concrete problem instances, we now present a more general mathematical formulation for the MIOCPs we have to solve, followed by a description of our numerical solution procedure.

We mathematically express our MIOCPs as

$$\min_{\substack{T,y,z \\ u_{\text{cont}},u_{\text{disc}}}} \quad \Phi\left(z(T)\right) \tag{16a}$$

$$\text{s.t.} \quad 0 = e(y, u_{\text{cont}}, u_{\text{disc}}), \tag{16b}$$

$$y(0,x) = y_0(x), \tag{16c}$$

$$\dot{z}(t) = f^{\text{ODE}}(t, z(t), y(t,\cdot), u_{\text{cont}}(t), u_{\text{disc}}(t)), \tag{16d}$$

$$z(0) = z_0, \tag{16e}$$

$$u_{\text{cont}}(t) \in \left[\underline{u_{\text{cont}}}, \overline{u_{\text{cont}}}\right], \tag{16f}$$

$$u_{\text{disc}}(t) \in \{u^1_{\text{disc}}, \ldots, u^{n_\omega}_{\text{disc}}\}, \tag{16g}$$

$$0 \leq G(z(t), u_{\text{cont}}(t), u_{\text{disc}}(t)). \tag{16h}$$

We briefly explain the occurring constraints in the above formulation. Constraints (16b) and (16c) represent the PDE model (1) with PDE states y and corresponding initial values. Moreover, we introduce an ODE constraint (16d) with states z and initial values given by (16e). The goal of this ODE system is to compute, for example, the amount of substances (12) or the control regularization terms that we introduce later. Hence the objective function (16a), which explicitly depends on the ODE states, represents both the control regularization, as well as the "actual" objective function (e.g. yield). Box constraints on the continuous controls $u_{\text{cont}} \in L^2(0,T)$ are given by (16f), and the discrete controls $u_{\text{disc}} \in L^\infty(0,T)$ must attain values in the set given in (16g). Finally, the inequality constraints (16h) shall represent, for example, bounds on yield and purity, but also reflect that some controls must be fixed during the feed inlet phase, compare (15c) and (15e). Therefore, the general inequality constraints G also represent equality constraints and point constraints (but for the sake of a simpler presentation). Note that the PDE states y neither enter the inequality constraints nor the objective function directly.

In order to solve (16), we employ a "first discretize, then optimize" strategy. This means that we first transform all infinite-dimensional quantities (PDE and ODE states, time-dependent controls) into finite representations, eventually yielding an NLP problem.

3.2.1. Spatial Discretization with WENO Scheme

First, we employ the method of lines approach (see e.g. Schiesser, 1991), i.e. we spatially discretize our PDE model (1). In our case, we employ a finite

volume method. To this end we introduce a (possibly non-uniform) spatial grid

$$0 = x_{1/2} < \cdots < x_{N+1/2} = L,$$

where the cells I_k and cell lengths Δx_k are given by

$$I_k := \left[x_{k-1/2}, x_{k+1/2}\right], \quad \Delta x_k := x_{k+1/2} - x_{k-1/2},$$

respectively, for $1 \leq k \leq N$. Afterwards, the states in our PDE model (1) are replaced by their cell averages

$$\bar{c}_k(t) := \frac{1}{\Delta x_k} \int_{x_{k-1/2}}^{x_{k+1/2}} c(t,x)\,\mathrm{d}x$$

and analogously for $\bar{c}_{p,k}$ and $\bar{q}_k$. Note that we drop the component subscript i in this paragraph for the sake of an uncluttered presentation; here, the subscript k denotes the respective cell I_k of the spatial grid.

Applying the operator $\int_{x_{k-1/2}}^{x_{k+1/2}} (\cdot)\,\mathrm{d}x$ to (1) for $1 \leq k \leq N$ and for a fixed $t \in (0,T)$, the PDE system is *approximated* by

$$\begin{aligned}
\frac{\mathrm{d}\bar{c}_k}{\mathrm{d}t}(t) = &- \frac{v_{\mathrm{sup}}}{\varepsilon_b} \frac{c(t,x_{k+1/2}) - c(t,x_{k-1/2})}{\Delta x_k} \\
&+ D_{\mathrm{ax}} \frac{\frac{\partial}{\partial x} c(t,x_{k+1/2}) - \frac{\partial}{\partial x} c(t,x_{k-1/2})}{\Delta x_k} \\
&- \frac{1-\varepsilon_b}{\varepsilon_b} \frac{3}{r_p} k_{\mathrm{eff},} \left(\bar{c}_k(t) - \bar{c}_{p,k}(t)\right), \\
\frac{\mathrm{d}\bar{c}_{p,k}}{\mathrm{d}t}(t) = &- \frac{(1-\varepsilon_p)}{\varepsilon_p} \frac{\mathrm{d}\bar{q}_k}{\mathrm{d}t}(t) + \frac{3}{\varepsilon_p r_p} k_{\mathrm{eff},} \left(\bar{c}_k(t) - \bar{c}_{p,k}(t)\right).
\end{aligned} \tag{17}$$

The boundary conditions (3) are incorporated by substituting

$$\begin{aligned}
&\frac{v_{\mathrm{sup}}}{\varepsilon_b} c(t,x_{1/2}) - D_{\mathrm{ax}} \frac{\partial c}{\partial x}(t,x_{1/2}) = \frac{v_{\mathrm{sup}}}{\varepsilon_b} c_{\mathrm{in}}(t), \\
&\frac{\partial c}{\partial x}(t,x_{N+1/2}) = 0.
\end{aligned}$$

Since the initial values (2) are independent of the spatial position x, they can be used as initial values for (17) without further modification.

The crucial point is the reconstruction of the cell interface values $c(t,x_{k+1/2})$ based on the given cell averages $\bar{c}_k(t)$; this is the actual approximation in (17). To this end, we apply a finite volume weighted essentially non-oscillatory (WENO) scheme, which has already been applied to a general rate model (GRM) for liquid chromatography on an equidistant spatial grid (von Lieres and Andersson, 2010). However, we apply the WENO scheme on a *non-uniform* grid for the following reasons: First of all, we are going to use lower order schemes close to the boundaries of the spatial grid, hence it is beneficial to control the error (particularly at column inlet) by choosing a finer grid size there. Moreover,

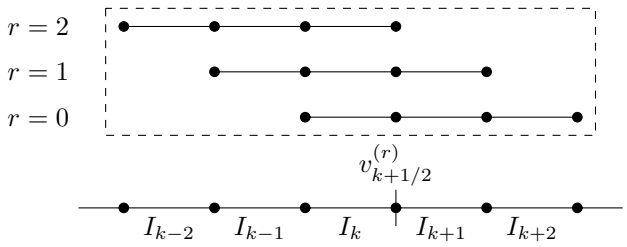

Figure 1: Schematic representation of stencils for the WENO35 scheme ($m = 3$).

despite the occurrence of a diffusion term in the PDE model (1), which dampens oscillations, the chromatography process is often convection-dominated. This, in combination with discontinuous inlet controls $c_{\mathrm{in},i}$, compare (15), can lead to instabilities when numerically solving the PDE. As an example, consider a change of pH from 4 to 8 (or vice versa). This corresponds to a change of the inlet concentration $c_{\mathrm{in,H^+}}$ from 10^{-4} to 10^{-8}. Even a small perturbation may lead to a negative concentration of protons close to column inlet. Clearly, the adsorption kinetics (10) can not be evaluated anymore, as the pH is defined as a logarithm of the proton concentration. Again, using a non-uniform grid gives us the possibility to control the error while using a reasonable total number of grid points.

The WENO method is a nonlinear high-order method originally designed for hyperbolic conservation laws. Its rationale is to obtain a high-order accuracy in regions where the solution of a PDE is smooth while also minimizing oscillatory behavior in regions where discontinuities occur. We only want to present the most fundamental ideas of this scheme and refer to Shu (1998, 2009) and the references cited therein for further information. Note that our description is limited to an upwind formulation for a *positive* flow velocity v_{sup}.

For the further presentation, let $\Delta x := \max_{1\le j\le N}\{\Delta x_j\}$ and let a piecewise smooth function $v : \mathbb{R} \to \mathbb{R}$ be given with cell averages

$$\bar{v}_k := \frac{1}{\Delta x_k} \int_{x_{k-1/2}}^{x_{k+1/2}} v(x)\,\mathrm{d}x, \tag{18}$$

for $1 \le k \le N$. Moreover, let m denote the desired order of accuracy. For $0 \le r \le m-1$, there are constants c_{rj}, $0 \le j \le m-1$, such that

$$v_{k+1/2}^{(r)} := \sum_{j=0}^{m-1} c_{rj}\bar{v}_{k-r+j} = v(x_{k+1/2}) + \mathcal{O}(\Delta x^m) \tag{19}$$

if v is sufficiently smooth on the stencil $\{I_{k-r}, \ldots, I_{k+m-1-r}\}$. Note that r represents the shift of the used stencil, compare Figure 1.

Furthermore, we have constants d_r, $0 \le r \le m-1$, such that

$$v_{k+1/2} := \sum_{r=0}^{m-1} d_r v_{k+1/2}^{(r)} = v(x_{k+1/2}) + \mathcal{O}(\Delta x^{2m-1}), \tag{20}$$

again, only if the function v is sufficiently smooth in the combined stencil $\{I_{k-m+1}, \dots, I_{k+m-1}\}$. However, in regions where discontinuities occur, this high-order *linear* scheme is likely to introduce oscillations in such regions, which is a reminiscence of Godunov's order barrier theorem (see e.g. Hesthaven, 2018).

Thus, the idea of the WENO method is to choose *nonlinear* weights w_r that give almost no weight to stencils where v is discontinuous, hence maintaining an accuracy of order m and also reducing oscillations. In smooth regions, these weights are chosen to achieve the high-order approximation of $2m-1$.

One possible way to define these weights for $0 \le r \le m-1$ is

$$w_r = \frac{a_r}{\sum_{l=0}^{m-1} a_l}, \qquad a_r = \frac{d_r}{(\varepsilon + \mathrm{IS}_r)^2}. \tag{21}$$

Here, ε is a small constant to circumvent a division by zero. It is often chosen as $\varepsilon = 10^{-6}$; alternatively it can be chosen to be dependent on the actual cell length Δx_k (compare Cravero and Semplice, 2016). The other quantity introduced in (21) are so-called smoothness indicators IS_r. These are computed as

$$\mathrm{IS}_r = \sum_{l=1}^{m-1} \int_{x_{k-1/2}}^{x_{k+1/2}} \Delta x_k^{2l-1} \left(\frac{\mathrm{d}^l}{\mathrm{d}x^l} \pi_r(x) \right)^2 \mathrm{d}x, \tag{22}$$

where π_r denotes the unique polynomial of degree at most $m-1$ that satisfies the approximation order property (19) with $v_{k+1/2}^{(r)} = \pi_r(x_{k+1/2})$. Furthermore, this polynomial reconstructs for $j \in \{k-r, \dots, k+m-1-r\}$ the cell averages $\bar{v}_j$,

$$\frac{1}{\Delta x_j} \int_{x_{j-1/2}}^{x_{j+1/2}} \pi_r(x) \, \mathrm{d}x = \bar{v}_j.$$

At this point we highlight the following crucial point: For a given spatial grid, most of the actual computation of the smoothness indicators (22) can be done independently of the actual cell average values $\bar{v}_j$. The same is true for the quantities c_{rj} and d_r, which depend on the actual grid, on the order m, and on the stencil shift r, but *not* on the actual function v or the respective cell averages. Hence, all these quantities can (and should be) computed beforehand. As long as the spatial grid is fixed, these quantities can be reused again. For a WENO23 ($m = 2$) and WENO35 ($m = 3$) scheme, formulas for the computation of all quantities are reported in the Appendix.

In order to apply the WENO scheme to our application, we simply have to replace $v(\cdot)$ by $c(t, \cdot)$ for a fixed time $t \in (0, T)$. We apply a WENO35 scheme for the reconstruction of the interface values for $x_{7/2} < \dots < x_{N-3/2}$, a WENO23 scheme for the points $\{x_{5/2}, x_{N-1/2}\}$, and a first-order upwind scheme for $\{x_{3/2}, x_{N+1/2}\}$. Finally, the remaining spatial derivatives in (17) are approximated by

$$\frac{\partial c}{\partial x}(t, x_{k+1/2}) \approx \frac{\bar{c}_{k+1}(t) - \bar{c}_k(t)}{0.5(\Delta x_k + \Delta x_{k+1})},$$

for $1 \le k \le N-1$. This way, all spatial derivatives occurring in (1) are replaced by (nonlinear) combinations of the cell averages.

After spatial discretization of the PDE model, we retrieve an ODE system with states y_h and corresponding right hand side f^{PDE}. The original PDE-constrained OCP (16) is thus transformed into an ODE-constrained OCP that can be expressed as

$$\min_{\substack{T, y_h, z \\ u_{\mathrm{cont}}, u_{\mathrm{disc}}}} \quad \Phi\left(z(T)\right) \tag{23a}$$

$$\text{s.t.} \quad \dot{y}_h(t) = f^{\mathrm{PDE}}(t, y_h(t), u_{\mathrm{cont}}(t), u_{\mathrm{disc}}(t)), \tag{23b}$$

$$y_h(0) = y_{h,0}, \tag{23c}$$

$$\dot{z}(t) = f^{\mathrm{ODE}}(t, z(t), y_h(t), u_{\mathrm{cont}}(t), u_{\mathrm{disc}}(t)), \tag{23d}$$

$$z(0) = z_0 \tag{23e}$$

$$u_{\mathrm{cont}}(t) \in \left[\underline{u_{\mathrm{cont}}}, \overline{u_{\mathrm{cont}}}\right], \tag{23f}$$

$$u_{\mathrm{disc}}(t) \in \{u^1_{\mathrm{disc}}, \ldots, u^{n_\omega}_{\mathrm{disc}}\}, \tag{23g}$$

$$0 \leq G(z(t), u_{\mathrm{cont}}(t), u_{\mathrm{disc}}(t)). \tag{23h}$$

Essentially, the original PDE constraint has been replaced by an ODE system. Furthermore, now the discretized states y_h enter the right-hand side f^{ODE}.

3.2.2. Partial Outer Convexification and Sum-Up Rounding

For an adequate treatment of the resulting ODE-constrained MIOCP, we perform a partial outer convexification and relaxation as described by e.g. Sager (2005); Sager et al. (2012) and Hante and Sager (2013). To this end, we introduce measurable binary controls $\omega : [0, T] \to \{0, 1\}^{n_\omega}$ and replace the right-hand sides in (23) by

$$\dot{y}_h(t) = \sum_{i=1}^{n_\omega} \omega_i(t) f^{\mathrm{PDE}}(t, y_h(t), u_{\mathrm{cont}}(t), u^i_{\mathrm{disc}}), \tag{24a}$$

$$\dot{z}(t) = \sum_{i=1}^{n_\omega} \omega_i(t) f^{\mathrm{ODE}}(t, z(t), y_h(t), u_{\mathrm{cont}}(t), u^i_{\mathrm{disc}}), \tag{24b}$$

thus replacing $u_{\mathrm{disc}}(t)$ by u^i_{disc} for $1 \leq i \leq n_\omega$. Furthermore, we additionally have to impose a special-ordered set of type 1 (SOS1) constraint on the binary controls,

$$1 = \sum_{i=1}^{n_\omega} \omega_i(t) \quad \text{for almost all } t \in [0, T]. \tag{25}$$

In a final step, the binary controls ω are replaced by relaxed counterparts $\alpha : [0, T] \to [0, 1]^{n_\omega}$. Hence, we arrive at a *continuous* ODE-constrained OCP.

Of course, an optimal solution of the *relaxed* problem is usually not an optimal solution for the *binary*, partially outer convexified OCP. Hence we apply the sum-up rounding (SUR) strategy described by Sager (2005); Sager et al. (2012) in order to transform the optimized relaxed controls α into binary-valued controls ω in a feasible way. To this end, assume we have a measurable

function $\alpha : [0,T] \to [0,1]^{n_\omega}$ that satisfies the SOS1 constraint, compare (25), and a time grid $0 = t_0 < \cdots < t_M = T$. Now define $\omega_i(t) := p_{i,j}$ for $t \in [t_j, t_{j+1})$, $1 \leq i \leq n_\omega$ and $0 \leq j < N$, where

$$p_{i,j} := \begin{cases} 1 & \text{if } \forall k \neq i \colon \hat{p}_{i,j} \geq \hat{p}_{k,j} \text{ and } \forall k \neq i,\ \hat{p}_{i,j} = \hat{p}_{k,j} \colon i < k, \\ 0 & \text{else,} \end{cases}$$

with $\hat{p}_{i,j}$ given by

$$\hat{p}_{i,j} := \int_0^{t_{j+1}} \alpha_i(\tau)\,\mathrm{d}\tau - \sum_{k=0}^{j-1} p_{i,k}(t_{k+1} - t_k).$$

It can be shown that the control function ω given by this procedure satisfies the SOS1 constraint. Furthermore, Kirches et al. (2020, Thm. 6.1) have shown the bound

$$\max_{t\in[0,T]} \left\| \int_0^t \alpha(\tau) - \omega(\tau)\,\mathrm{d}\tau \right\|_\infty \leq h \sum_{i=2}^{n_\omega} \frac{1}{i} \in \mathcal{O}(h \log(n_\omega)),\ h := \max_{0\leq j<N} \{t_{j+1} - t_j\}.$$

Note that the right side of this inequality can be made arbitrarily small by choosing a sufficiently small time (rounding) grid. This way, the absolute error between the objective value for the relaxed and the binary partially outer convexified OCP can be made arbitrarily small (Kirches et al., 2020, Thm. 3.6). If the discrete controls do *not* enter directly, the same is true for the inequality constraint function, compare (16h). Hence, partial outer convexification yields a tight relaxation. Note, however, that choosing a fine rounding grid may lead to frequently switching rounded controls. To overcome this issue, one could for example determine the rounded controls by solving a mixed-integer linear programming (MILP) problem that limits the number of switches (compare Sager et al., 2011; Belotti et al., 2013; Bestehorn et al., 2019, 2020).

For our OCPs (13) and (14) and the corresponding MIPDECO problem (16), we must emphasize an important caveat: Since the pH must be kept constant during the feed inlet phase, it is not desirable to make the rounding grid arbitrarily small to control the relaxation error during this time period. A possibility to overcome this issue is to solve a small number of OCPs corresponding to the number of attainable pH values and where the initial pH is fixed during the inlet phase. Afterwards, we choose the best solution out of all these solved OCPs. As this constraint is the only reason why the discrete controls enter the inequality constraint (16h) directly, feasibility of all other constraints that we introduced so far (e.g. purity requirements) is approximated arbitrarily well after rounding. For the general situation of constraints depending on the integer control, we refer to Kirches et al. (2020).

Finally, we remark that if $\mathrm{coll}(t)$ is the only discrete process control and if it enters the right-hand sides in (23) linearly (which is the case for our OCP examples), then the ODE-constrained MIOCP is already partially outer convexified.

3.2.3. Control Discretization with Direct Single Shooting Approach

Let us now take a step back to the point where the OCP is partially outer convexified and relaxed. In order to transform this continuous ODE-constrained OCP into an NLP problem, we apply a direct single shooting method. To this end, we introduce a control grid with grid points $0 = t_0 < \cdots < t_M = T$. On each control interval $[t_j, t_{j+1})$ the continuous controls u_{cont} are represented by a finite parameterization. For example, we can use piecewise polynomials and hence the optimization variables are the coefficients of these polynomials. Of course, the continuous controls $\alpha(t)$ introduced by the partial outer convexification and relaxation should be treated as piecewise constant. The ODE state trajectories are then assumed to be dependent values on the controls and the initial values.

Direct single shooting is often used in practice, as it is a rather intuitive approach and easy to implement. However, this method suffers from some drawbacks that we do not want to hide. For example, a solution of an initial value problem does not even have to exist if the initial controls are chosen poorly. Even if a solution exists, obtaining an optimal solution might only be possible if we start already close to it, especially if the underlying system is highly nonlinear. In order to overcome these issues, Bock and coworkers developed the so-called direct multiple shooting method, see e.g. the seminal paper by Bock and Plitt (1984), which improves upon stability and has successfully been applied to many applications (see e.g. Diehl et al., 2002; Leineweber et al., 2003; Kirches, 2011, and the references cited therein). However, we do not discuss this method further and refer the reader to the respective literature instead.

Having applied the direct single shooting method, thus replacing the infinite-dimensional optimization quantities by a finite representation (initial values and discretized controls), we can transform the OCP into a NLP problem which can be solved by, for example, a sequential quadratic programming (SQP) or interior point method (see Nocedal and Wright, 2006).

3.3. Regularization of Process Controls

So far, we have introduced concrete OCP instances for column liquid chromatography and we have discussed a numerical solution strategy for the underlying MIPDECO problems. We now draw our attention to a subtle problem. Suppose there is some time $T^* \in (0, T)$ such that all components have left the column when reaching T^*. Then, for the remaining time $t \in (T^*, T]$, the process controls are likely to have no impact on the objective function anymore. The same may hold at the very beginning of the process: Since it takes some time for the components to flow through the column, it does not matter what value the collect control $\text{coll}(t)$ has, as there is no eluate flowing out of the column. In both cases, we face the same problem: Some (or all) of the controls are not uniquely determinable for certain time horizons, possibly leading to degenerate systems within the numerical optimization procedure.

To overcome this issue, we *regularize* the (free) process controls, meaning that we "push" the controls to a certain reference value if they have no impact on the objective and constraints. For a continuous control we use an L^2

regularization term, i.e. we integrate over the squared deviation of a control to its desired reference value. For a discrete control we use an L^1 regularization, thus integrating the absolute value of the deviation of a discrete control to its reference value. Hence, we expand the objective function by adding

$$\sum_{j=1}^{n_{\text{cont}}} \int_0^T \left(u_{\text{cont,j}}(\tau) - u_{\text{cont,ref,j}}\right)^2 \mathrm{d}\tau + \sum_{j=1}^{n_{\text{disc}}} \int_0^T \left|u_{\text{disc,j}}(\tau) - u_{\text{disc,ref,j}}\right| \mathrm{d}\tau.$$

We note that the L^1 and L^2 regularization terms fit into our problem formulation (16) by introduction of additional ODE states whose right-hand side is the integrand of the respective norm. The right-hand sides should additionally be weighted by a small factor, ensuring that the regularization term does not dominate the actual objective function (e.g. maximizing the yield). For a discussion of regularization in the context of MIOCP, we also refer to (Manns and Kirches, 2018).

Moreover, the reference values $u_{\star,\text{ref},j}$ should reflect a *desired* behavior. For example, one would typically choose a low salt concentration as a reference value since this is cheaper than using buffers with high salt concentration. Furthermore, the reference pH can be chosen to create a mild environment for the chromatographic resin. Of course, there is no guarantee that the respective reference values are reached at the end of the (optimization) process. If a certain value must be achieved, additional constraints must be added to the OCP formulation.

Finally, note that the advantage of using an L^1 regularization for the discrete controls is that a possible "bang-bang" behavior for these (optimized) controls is preserved. Using an L^2 regularization often destroys this property. The disadvantage is that the integrand is is not differentiable anymore, which may cause difficulties for the employed NLP solver.

4. Computational Results

We now apply the previously described strategies to solve the OCPs (13) and (14). First, we present the setup for our computational experiments by describing, among other things, the used software, model parameters, and employed discretization grids. Afterwards, we present and discuss the solutions obtained with our numerical procedure.

4.1. Computational Setup

As a computational framework we use CasADi (Andersson et al., 2019), which is a tool for automatic differentiation and derivative-based numerical optimization. All the derivatives needed to eventually create the NLP problem are provided by CasADi and its interfaced ODE integrators. For further information, including concrete examples on how to transform an OCP into an NLP problem by means of e.g. the single shooting method, we refer to the code templates provided by the CasADi developers. As an integrator we use CasADi's

Table 1: Options used for IDAS and IPOPT.

	Option name	Value
IDAS	`reltol`	10^{-6}
	`abstol`	10^{-11}
	`max_num_steps`	10^{6}
	`max_order`	3
IPOPT	`limited_memory_max_history`	20
	`compl_inf_tol`	10^{-6}
	`constr_viol_tol`	10^{-6}
	`dual_inf_tol`	$2.5 \cdot 10^{-3}$
	`tol`	$2.5 \cdot 10^{-3}$
	`max_iter`	150

interface to IDAS (Hindmarsh et al., 2005) and the NLP problem is solved by IPOPT (Wächter and Biegler, 2006) using a limited-memory BFGS approximation for the Hessian (Nocedal and Wright, 2006). We use the default options for the integrator and the NLP solver, except for the quantities reported in Table 1. The prototypical implementation was done in MATLAB.

We use the model parameters reported in Table 2; note that we employ the commonly used unit $\mathrm{M} = \mathrm{mol\,L^{-1}}$ for the molar concentration. The impurity is represented by the *first* component and the product is given by the *second* component. The parameter values do not reflect a specific MMC resin or specific proteins; however they are chosen in a way to reflect typical values as reported by various others (Nfor et al., 2010; Deitcher et al., 2010; Schmidt-Traub et al., 2012). For example, the values of model parameters given in (1) are in a typical range described by Schmidt-Traub et al. (2012), the value for ρ in (10) has been taken from Jenkins (1998) for sodium chloride, the value of ξ reflects a butyl functional group reported by Deitcher et al. (2010), and the effective mass transfer coefficient for salt ($k_{\mathrm{eff,salt}}$) is also used by Benner et al. (2019). The parameters $\nu_{i,1}$ and $\nu_{i,2}$ are chosen such that the binding charges of both components as given by (11) are almost equal for a pH of 4, but the corresponding equilibrium parameters $k_{\mathrm{eq},i}$ "shift" to different directions for this pH due to opposite signs of the weighting factor $\gamma_{\mathrm{pH},i}$.

The grid for the spatial discretization consists of $N = 69$ cells. We choose the cell lengths Δx_k as

$$\Delta x_k = L \cdot \begin{cases} 10^{-3} & \text{for } 1 \leq k \leq 10, \\ 10^{-3} + (k-11)10^{-3} & \text{for } 11 \leq k \leq 30, \\ 2 \cdot 10^{-2} & \text{for } 31 \leq k \leq 69. \end{cases}$$

We furthermore use an equidistant control grid for each experiment, every interval having a length of $\Delta t = 0.5\,\mathrm{min}$. Note that the grid is fixed within the feed inlet phase, but optimizing the batch-cycle time is likely to alter the interval length of the grid after feed inlet.

Table 2: Model parameters for computational experiments.

Symbol	Value	Unit	Symbol	Value	Unit
L	25	mm	D_{ax}	2.0	$\mathrm{mm^2\,min^{-1}}$
ε_b	0.35	–	$k_{\mathrm{eff,H^+}}$	1.5	$\mathrm{mm\,min^{-1}}$
r_p	0.04	mm	$k_{\mathrm{eff,salt}}$	1.5	$\mathrm{mm\,min^{-1}}$
ε_p	0.9	–	$k_{\mathrm{eff},1/2}$	0.5 / 0.2	$\mathrm{mm\,min^{-1}}$
$k_{\mathrm{eq},0,1/2}$	1.0 / 2.0	–	$k_{\mathrm{kin},1/2}$	$2 \cdot 10^4$ / 10^4	$\mathrm{M^{-\nu_i\,-\,n_i}\,min^{-1}}$
$\gamma_{\mathrm{pH},1/2}$	0.1 / -0.3	–	$\nu_{1/2,1}$	0.5 / -0.2	–
$\nu_{1/2,2}$	2.5 / 3.5	–	$\varsigma_{1/2}$	75 / 100	–
Λ_{IEX}	0.8	M	$n_{1/2}$	1.0 / 2.0	–
$\delta_{1/2}$	75 / 100	–	$\tilde{c}$	1.0	M
Λ_{HIC}	0.8	M	ξ	16	–
ρ	-0.015	$\mathrm{M^{-1}}$	$\kappa_{\mathrm{salt},1/2}$	1.0 / 2.0	$\mathrm{M^{-1}}$

The bounds on the controls and their reference values for the regularization (of free controls) are given as follows: We use a *fixed* volumetric flow rate $\dot{V} = 0.5{\cdot}10^{-3}\,\mathrm{L\,min^{-1}}$, which corresponds to a superficial flow velocity v_{sup} of roughly $25\,\mathrm{mm\,min^{-1}}$. The feed load concentrations are the same for both components, namely $c_{\mathrm{load},1/2} = 10^{-6}\,\mathrm{M}$. The range for the salt inlet is $c_{\mathrm{in,salt}}(t) \in [0.1, 1.0]$ and its reference value is 0.1 M. Furthermore, for the inlet concentration of protons (i.e. possible pH values) we choose $c_{\mathrm{in,H^+}}(t) \in \{10^{-8}, 10^{-4}\}$ and the corresponding reference value is $10^{-8}\,\mathrm{M}$. The reference value for the binary collect control is 0. Finally, note that the initial concentrations $c_{\mathrm{salt,init}}$ and $\mathrm{pH_{init}}$ have the same bounds as their corresponding control functions $c_{\mathrm{in,salt}}(t)$ and $c_{\mathrm{in,H^+}}(t)$, respectively. The reference value $\mathrm{pH_{ref}}$ for the MMC kinetics (11) is in accordance with the reference value for the proton inlet concentration, hence $\mathrm{pH_{ref}} = 8$.

4.2. Results and Discussion

For the case studies, we use $c_{\mathrm{in,salt}}(t) = 0.5\,\mathrm{M}$ and $\mathrm{coll}(t) = 1$ for $t \in [0, T]$ as an initial guess. Moreover, each OCP is solved twice: once for $\mathrm{pH_{in}}(t) = 4$ and once for $\mathrm{pH_{in}}(t) = 8$ for $t \in [0, T]$, where $\mathrm{pH_{in}}(t) := -\log_{10} c_{\mathrm{in,H^+}}(t)$. The respective pH must then stay fixed during the inlet phase. We use a fixed inlet time $t_{\mathrm{in}} = 1\,\mathrm{min}$ and the (initial guess for the) end time is $T = 6\,\mathrm{min}$. Given these process controls, the resulting concentration profiles at column outlet (for a longer time horizon) are depicted in Figure 2. There, we can see that the impurity is only mildly affected by different initial pH values. However, the product is strongly affected. On the one hand, for a pH of 4 the product elutes over a long time horizon, which is certainly not a desired behavior. On the other hand, for a pH of 8 the overlap of impurity and product is rather high, so no good separation is achieved. Since we choose the final time as $T = 6\,\mathrm{min}$, the goal of the optimization procedure must be to obtain a much sharper elution

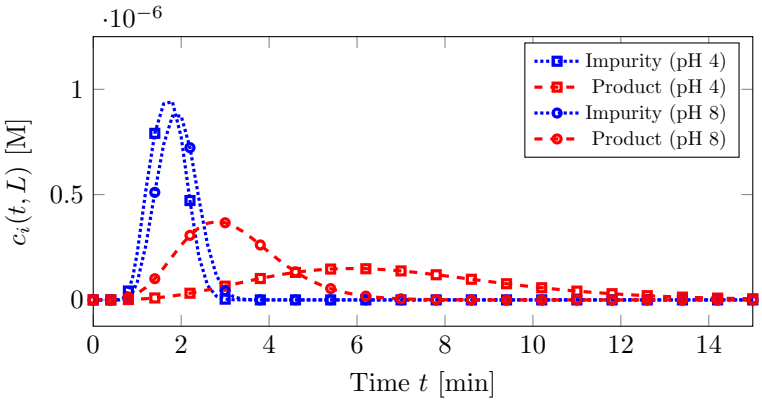

Figure 2: Concentration profiles obtained for the initial control trajectories.

profile for the product that also has just very few (if any) overlap with the impurity.

Case 1: Maximize Yield with Fixed End Time

This case corresponds to OCP (13). In addition to the aforementioned initial setup, we enforce for each component that 98.5% of the injected amount of substance is eluted after optimization. Hence, with the definition in OCP (13), we have $\zeta_i = 0.985$ for $i \in \{1, 2\}$. We perform multiple experiments for different lower bounds on the purity of the product. More specifically we enforce a purity of 90%, 95%, and 99%, respectively.

For a piecewise linear salt inlet trajectory and an initial pH of 4, the optimized yield ranges from approximately 99.4% for a minimum purity of 90% to 98.9% for a minimum purity of 99%. Using an initial pH of 8, the yield ranges from 99.4% to 97.9% for the respective purity requirements. Hence we see that there is no big difference in the optimized yields, but an initial pH of 4 is slightly more beneficial. The corresponding concentration profiles and control trajectories for a minimum purity of 99% are depicted in Figure 3. There, we can see that the product and impurity are almost completely eluted within the prescribed time horizon. Moreover, the components are nearly fully separated from each other. The collect control is already binary without rounding, but we must apply the SUR strategy for the pH (dotted line). We notice, however, that there is no constraint violation and no loss in yield after rounding, so the "kink" in the pH trajectory may also be attributable to an immature termination of the NLP solver due to the chosen termination criteria.

For a piecewise constant salt inlet trajectory we observe a bigger difference for different initial pH values. For $\mathrm{pH}_{\mathrm{init}} = 4$, the optimized yield ranges from approximately 99.4% for a minimum purity of 90% to 96.4% for a minimum purity of 99%. Using an initial pH of 8, the yield ranges from 98.9% to 90.6% for the respective purity constraints. Thus, an initial pH of 4 is clearly the better choice. The corresponding concentration profiles and control trajectories for a

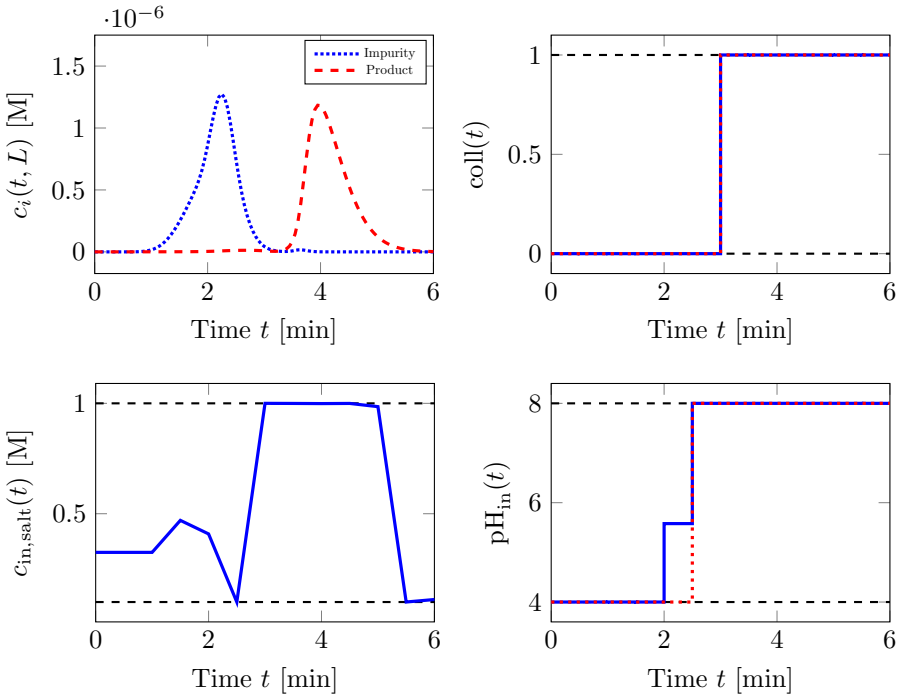

Figure 3: Optimized concentration profiles and control trajectories for $\text{Purity}_{\text{min},*} = 0.99$, $\text{pH}_{\text{init}} = 4$, and piecewise linear salt inlet. Dashed lines within control plots represent the box constraints, dotted trajectories are obtained by SUR.

minimum purity of 99% are depicted in Figure 4. We highlight that the elution peaks are located earlier in time compared to using a piecewise linear salt inlet trajectory; especially the impurity elutes much earlier and has a sharper profile. We furthermore see that the product and impurity are also well separated, but not quite as good as when using a piecewise linear salt trajectory (note the small "bump" of the product within the impurity peak). Moreover, the pH and collect control are almost discrete valued without applying the SUR strategy. Consequently, there is no constraint violation or loss in the objective function after rounding.

Using a *fixed* pH of 8 over the whole time horizon and having a purity requirement of 99%, we achieve a yield of roughly 70% for a piecewise linear salt inlet trajectory and a yield below 60% for a piecewise constant salt inlet. For a fixed pH of 4, we achieve a yield of slightly more than 93% independent of the actual parameterization of the salt inlet. Hence a pH of 8 is definitely not a good choice, but a pH of 4 gives comparable results.

All in all, we note that in most cases a feasible solution for the original MIOCPs can be achieved even without applying a rounding scheme; this is also true for $\text{pH}_{\text{init}} = 8$ and lower purity requirements (results not shown). However,

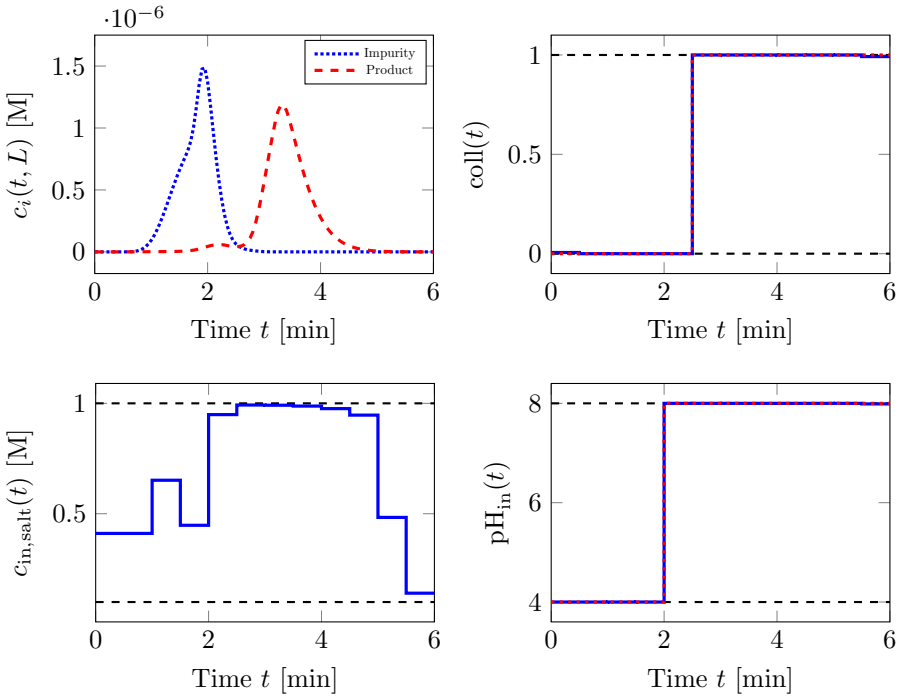

Figure 4: Optimized concentration profiles and control trajectories for $\text{Purity}_{\text{min},*} = 0.99$, $\text{pH}_{\text{init}} = 4$, and piecewise constant salt inlet. Dashed lines within control plots represent the box constraints, dotted trajectories are obtained by SUR.

we observed that using an L^2 regularization for the discrete process controls may violate this behavior, and that using an L^1 regularization is recommended for these controls even if non-differentiability is introduced.

Case 2: Minimize Batch-cycle Time

This case corresponds to OCP (14). We us the same (initial) setup as in the first case study before; additionally we set $\text{Yield}_{\text{min},*} = 0.95$, hence our goal is to obtain at least a yield of 95%. As the end time is subject to optimization, we impose bounds given by $T \in [2, 15]$.

For a piecewise linear salt inlet and an initial pH of 4, the optimized end times range from $T \approx 3.8$ for 90% purity to $T \approx 4.66$ for 99% purity. For a piecewise constant salt inlet, the end times range from $T \approx 3.79$ for 90% purity to $T \approx 4.29$ for 99% purity. We therefore note that a piecewise constant representation of the salt inlet gives better results than a piecewise linear representation. For a desired purity of 99% and an initial pH of 4, the concentration profiles and control trajectories are depicted in Figures 5 and 6.

As was the case when maximizing the yield, using a piecewise constant salt inlet trajectory leads to sharper peaks, especially for the impurity. This also explains the better batch-cycle time.

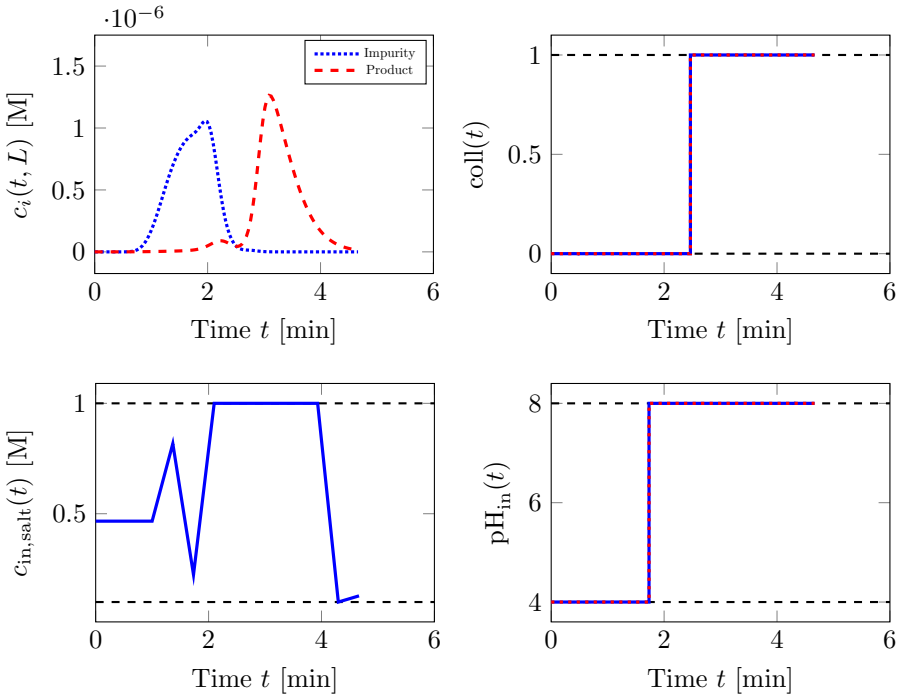

Figure 5: Optimized concentration profiles and control trajectories for $\text{Purity}_{\text{min},*} = 0.99$, $\text{pH}_{\text{init}} = 4$, and piecewise linear salt inlet. Dashed lines within control plots represent the box constraints, dotted trajectories are obtained by SUR.

The optimized batch-cycle times were always worse when using an initial pH of 8. On average, the optimized end time was approximately 0.4 min higher compared to using $\text{pH}_{\text{init}} = 4$.

We furthermore compared our solutions to setups where the pH was fixed. For a purity requirement of 99% and having $\text{pH} = 8$, the optimization problem could not be solved. This is probably because the OCP was not feasible for the given lower bounds on yield and purity (we have seen in the previous section that we could only achieve a yield of less than 70% for a minimum purity of 99% and a fixed end time $T = 6$). Using a fixed pH of 4 and enforcing a minimum purity of 99% we get an optimized end time $T \approx 6.16$ for a piecewise constant salt inlet and we have $T \approx 6.28$ for a piecewise linear salt inlet. We thus lose nearly two minutes when using a constant pH compared to being able to switch between prescribed pH values. This signifies the importance of incorporating the pH as an additional quantity for the MMC kinetics.

Finally, we note that the optimized pH and collect trajectories were almost always feasible for the original MIOCPs. Thus, rounding had almost no effect and neither loss in the objective function nor a constraint violation occurs.

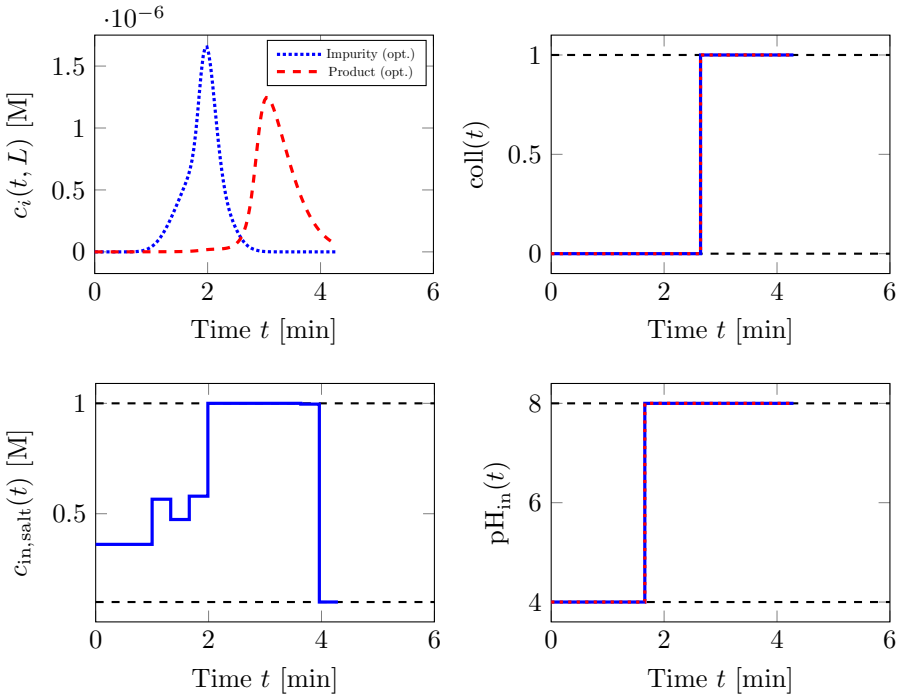

Figure 6: Optimized concentration profiles and control trajectories for $\text{Purity}_{\text{min},*} = 0.99$, $\text{pH}_{\text{init}} = 4$, and piecewise constant salt inlet. Dashed lines within control plots represent the box constraints, dotted trajectories are obtained by SUR.

5. Conclusion and Extensions

We presented a fairly general mathematical framework for the optimization of column liquid chromatography processes, here applied to a challenging MMC application. To this end, we employed a transport dispersive (lumped pore) model with a recent highly nonlinear adsorption kinetics for MMC, the latter taking both buffer salt concentration and pH into account. Here, the pH was assumed to be a discrete process control, as was an additional control that signifies whether the eluate collection is turned off or on. We gave a step-by-step description on how to solve the resulting MIPDECO problems.

We introduced two specific OCPs, one that maximizes the yield of the product and one that minimizes the batch-cycle time. The product had to fulfill a purity requirement and the column had to be (nearly) completely emptied from all components at the end of the purification process. We showed that, under the given experimental setup, a good separation could be achieved in a two-component system, even for high purity requirements. Furthermore, we have seen that the pH plays an important role for the purification process, especially when the task is to minimize the batch-cycle time. In nearly all examined cases, we observed a bang-bang behavior for the optimized, originally discrete, process

controls. In cases where no bang-bang behavior was observed, the constraint violation and the loss in the objective value after rounding of the controls were negligible.

All in all, the proposed framework is very flexible in that it covers the incorporation of multiple optimization criteria (as objectives and/or constraints), as well as continuous and discrete process controls. Modeling the eluate collection as an additional control instead of cut points for a single collect interval further increases the flexibility. Of course, our framework can be used for other types of column liquid chromatography processes by using different models for the column and/or adsorption behavior.

One possible extension, which also fits into our framework, is the incorporation of additional tubing before the column, as this reflects the actual design of several chromatography systems. An instationary convection-diffusion PDE model is often used to account for tubing (Schmidt-Traub et al., 2012); however, an additional PDE system will of course increase the overall problem dimension after discretization. Another interesting extension is the following: In most chromatography systems the flow direction can be reversed. This is done to obtain sharper elution profiles, as the desired product does not have to flow through the whole column then. Hence we are searching for an optimal "switching point" for the flow reversal. This is not a trivial task, one reason being that the spatial discretization of the chromatography column must be adapted in order to be an upwind scheme for the sake of numerical stability. To incorporate such a determination of an optimal switching point can be beneficial in some column chromatography applications.

Acknowledgments

All authors gratefully acknowledge support by the German Federal Ministry for Education and Research under grants MOPhaPro (05M16VHA, 05M17MBA). The first, third, and fourth author also gratefully acknowledge support by the German Federal Ministry for Education and Research under grant MOReNet (05M18VHA). The first and third author gratefully acknowledge support by the German Research Foundation within the priority program DFG-SPP 1962.

Appendix

Coefficients for WENO23 Scheme

Here, $m = 2$ and we seek a reconstruction of $v_{k+1/2}$ for a fixed k. For the sake of a simpler notation we introduce cell lengths $h_l = \Delta x_{k-2+l}$ for $1 \leq l \leq 3$. Furthermore, we have $0 \leq r, j \leq 1$. We mainly follow the presentation given by Wang et al. (2008), who derive the necessary formulas for the WENO35 scheme (presented afterwards).

For the coefficients c_{rj}, compare (19), we have $c_{rj} = h_{2-r+j}\, b_{rj}$, the latter given by

$$b_{01} = \frac{h_2}{(h_2 + h_3)h_3},$$

$$b_{00} = b_{01} - \frac{h_2 - h_3}{h_2 h_3},$$
$$b_{11} = \frac{h_1 + 2h_2}{(h_1 + h_2)h_2},$$
$$b_{10} = b_{11} - \frac{h_1 + h_2}{h_1 h_2}.$$

Furthermore, the coefficients d_r, compare (20), are given by

$$d_0 = \frac{h_1 + h_2}{h_1 + h_2 + h_3},$$
$$d_1 = \frac{h_3}{h_1 + h_2 + h_3}.$$

Finally, we note that $\pi_r^{'}$ is a constant polynomial, hence it can be expressed as

$$\pi_r^{'} = \sum_{j=0}^{1} h_{2-r+j} B_{rj}^{'} \bar{v}_{k-r+j},$$

with constant coefficients $B_{rj}^{'}$ given by

$$B_{01}^{'} = \frac{2}{(h_2 + h_3)h_3},$$
$$B_{00}^{'} = B_{01}^{'} - \frac{2}{h_2 h_3},$$
$$B_{11}^{'} = \frac{2}{(h_1 + h_2)h_2},$$
$$B_{10}^{'} = B_{11}^{'} - \frac{2}{h_1 h_2}.$$

For the smoothness indicators (22) we thus have

$$\mathrm{IS}_r = (h_2)^2 \left(\sum_{j=0}^{1} h_{2-r+j} B_{rj}^{'} \bar{v}_{k-r+j} \right)^2.$$

Coefficients for WENO35 Scheme

Here, $m = 3$ and we seek a reconstruction of $v_{k+1/2}$ for a fixed k. The cell lengths are now given as $h_l = \Delta x_{k-3+l}$ for $1 \le l \le 5$. Moreover, we have $0 \le r, j \le 2$. The following presentation and the reported values are mainly taken from Wang et al. (2008).

For the coefficients c_{rj}, compare (19), we have $c_{rj} = h_{3-r+j}\, b_{rj}$, the latter given by

$$b_{02} = \frac{-h_3 h_4}{(h_3 + h_4 + h_5)(h_4 + h_5)h_5},$$

$$
\begin{aligned}
b_{01} &= b_{02} + \frac{h_3(h_4+h_5)}{(h_3+h_4)h_4h_5},\\
b_{00} &= b_{01} + \frac{1}{h_3} - \frac{1}{h_4} - \frac{1}{h_4+h_5},\\
b_{12} &= \frac{(h_2+h_3)h_3}{(h_2+h_3+h_4)(h_3+h_4)h_4},\\
b_{11} &= b_{12} + \frac{1}{h_2+h_3} + \frac{1}{h_3} - \frac{1}{h_4},\\
b_{10} &= b_{11} - \frac{(h_2+h_3)h_4}{h_2h_3(h_3+h_4)},\\
b_{22} &= \frac{1}{h_1+h_2+h_3} + \frac{1}{h_2+h_3} + \frac{1}{h_3},\\
b_{21} &= b_{22} - \frac{(h_1+h_2+h_3)(h_2+h_3)}{(h_1+h_2)h_2h_3},\\
b_{20} &= b_{21} + \frac{(h_1+h_2+h_3)h_3}{h_1h_2(h_2+h_3)}.
\end{aligned}
$$

Now, let $H_{l_1}^{l_2} := \sum_{l=l_1}^{l_2} h_l$. The coefficients d_r, compare (20), are then given by

$$
\begin{aligned}
d_0 &= \frac{H_2^3 H_1^3}{H_1^5 H_2^5},\\
d_1 &= \frac{H_1^3 H_4^5}{H_1^4 H_2^5 H_1^5}(h_1+2h_2+2h_3+2h_4+h_5),\\
d_2 &= h_4 \frac{H_4^5}{H_1^4 H_1^5}.
\end{aligned}
$$

The smoothness indicators (22) can be computed as follows: First, we note that $\pi_r^{''}$ is a constant polynomial, hence it can be expressed as

$$
\pi_r^{''} = \sum_{j=0}^{2} h_{3-r+j} B_{rj}^{''} \bar{v}_{k-r+j},
$$

with constant coefficients $B_{rj}^{''}$ given by

$$
\begin{aligned}
B_{r2}^{''} &= \frac{6}{(h_{3-r}+h_{4-r}+h_{5-r})(h_{4-r}+h_{5-r})h_{5-r}},\\
B_{r1}^{''} &= B_{r2}^{''} - \frac{6}{(h_{3-r}+h_{4-r})h_{4-r}h_{5-r}},\\
B_{r0}^{''} &= B_{r1}^{''} + \frac{6}{h_{3-r}h_{4-r}(h_{4-r}+h_{5-r})}
\end{aligned}
$$

for $0 \le r \le 2$. Hence, the second integral in (22) becomes

$$
\int_{x_{k-1/2}}^{x_{k+1/2}} (h_3)^3 \left(\pi_r^{''}(x)\right)^2 \mathrm{d}x = (h_3)^4 \left(\sum_{j=0}^{2} h_{3-r+j} B_{rj}^{''} \bar{v}_{k-r+j} \right)^2.
$$

Furthermore, $\pi_r^{'}$ is a linear polynomial and hence $(\pi_r^{'})^2$ is quadratic in x. We therefore apply Simpson's rule to exactly integrate this polynomial. To this end, we set

$$\pi_r^{'}(x) = \sum_{j=0}^{2} h_{3-r+j} B_{rj}^{'}(x) \bar{v}_{k-r+j}$$

and compute the coefficients $B_{rj}^{'}(x)$ for the points $x_{k-1/2}$, $x_{k+1/2}$, and $x_k = \frac{1}{2}\left(x_{k-1/2} + x_{k+1/2}\right)$,

$$\begin{aligned}
B_{02}^{'}(x_{k-1/2}) &= \frac{-2(2h_3+h_4)}{(h_3+h_4+h_5)(h_4+h_5)h_5},\\
B_{01}^{'}(x_{k-1/2}) &= B_{02}^{'}(x_{k-1/2}) + \frac{2(2h_3+h_4+h_5)}{(h_3+h_4)h_4h_5},\\
B_{00}^{'}(x_{k-1/2}) &= B_{01}^{'}(x_{k-1/2}) - \frac{2(2h_3+2h_4+h_5)}{h_3h_4(h_4+h_5)},\\
B_{12}^{'}(x_{k-1/2}) &= \frac{2(h_2-h_3)}{(h_2+h_3+h_4)(h_3+h_4)h_4},\\
B_{11}^{'}(x_{k-1/2}) &= B_{12}^{'}(x_{k-1/2}) - \frac{2(h_2-h_3-h_4)}{(h_2+h_3)h_3h_4},\\
B_{10}^{'}(x_{k-1/2}) &= B_{11}^{'}(x_{k-1/2}) + \frac{2(h_2-2h_3-h_4)}{h_2h_3(h_3+h_4)},\\
B_{22}^{'}(x_{k-1/2}) &= \frac{2(h_1+2h_2)}{(h_1+h_2+h_3)(h_2+h_3)h_3},\\
B_{21}^{'}(x_{k-1/2}) &= B_{22}^{'}(x_{k-1/2}) - \frac{2(h_1+2h_2-h_3)}{(h_1+h_2)h_2h_3},\\
B_{20}^{'}(x_{k-1/2}) &= B_{21}^{'}(x_{k-1/2}) + \frac{2(h_1+h_2-h_3)}{h_1h_2(h_2+h_3)},\\
B_{rj}^{'}(x_k) &= B_{rj}^{'}(x_{k-1/2}) + \frac{1}{2}h_3 B_{rj}^{''},\\
B_{rj}^{'}(x_{k+1/2}) &= B_{rj}^{'}(x_{k-1/2}) + h_3 B_{rj}^{''},
\end{aligned}$$

the latter two equations holding for $0 \le r, j \le 2$. Applying Simpson's rule, we obtain for the first integral in (22)

$$\begin{aligned}
&\int_{x_{k-1/2}}^{x_{k+1/2}} h_3 \left(\pi_r^{'}(x)\right)^2 \mathrm{d}x\\
&\qquad = \frac{(h_3)^2}{6}\left(\left(\pi_r^{'}(x_{k-1/2})\right)^2 + 4\left(\pi_r^{'}(x_k)\right)^2 + \left(\pi_r^{'}(x_{k+1/2})\right)^2\right).
\end{aligned}$$

The smoothness indicators can then be computed by combining both of the above defined integrals. Note that all coefficients must only be computed once as long as the grid stays fixed.

References

Andersson, J.A.E., Gillis, J., Horn, G., Rawlings, J.B., Diehl, M., 2019. CasADi: a software framework for nonlinear optimization and optimal control. Math. Prog. Comp. 11, 1–36.

Behrens, M., Khobkhun, P., Potschka, A., Engell, S., 2014. Optimizing set point control of the MCSGP process, in: 2014 European Control Conference (ECC), Strasbourg, France. pp. 1139–1144.

Belotti, P., Kirches, C., Leyffer, S., Linderoth, J., Luedtke, J., Mahajan, A., 2013. Mixed-integer nonlinear optimization. Acta Numer. 22, 1–131.

Benner, S.W., Welsh, J.P., Rauscher, M.A., Pollard, J.M., 2019. Prediction of lab and manufacturing scale chromatography performance using mini-columns and mechanistic modeling. J. Chromatogr. A 1593, 54–62.

Bestehorn, F., Hansknecht, C., Kirches, C., Manns, P., 2019. A switching cost aware rounding method for relaxations of mixed-integer optimal control problems, in: 2019 IEEE 58th Conference on Decision and Control (CDC), Nice, France. pp. 7134–7139.

Bestehorn, F., Hansknecht, C., Kirches, C., Manns, P., 2020. Mixed-integer optimal control problems with switching costs: A shortest path approach. Math. Progam. Ser. B URL: `http://www.optimization-online.org/DB\_HTML/2020/02/7630.html`. (Submitted).

Bock, H.G., Plitt, K.J., 1984. A multiple shooting algorithm for direct solution of optimal control problems. IFAC Proceedings Volumes 17, 1603–1608. 9th IFAC World Congress: A Bridge Between Control Science and Technology, Budapest, Hungary, 2-6 July 1984.

Brooks, C.A., Cramer, S.M., 1992. Steric mass-action ion exchange: Displacement profiles and induced salt gradients. AIChE J. 38, 1969–1978.

Buchheim, C., Kuhlmann, R., Meyer, C., 2018. Combinatorial optimal control of semilinear elliptic pdes. Comput. Optim. Appl. 70, 641–675.

Cebulla, D.H., Kirches, C., Potschka, A., 2019. Parameter identifiability in a novel kinetic adsorption isotherm for multi-modal chromatography, in: 2019 IEEE 58th Conference on Decision and Control (CDC), Nice, France. pp. 4755–4760.

Cebulla, D.H., Kirches, C., Potschka, A., 2020. Mixed-integer nonlinear PDE-constrained optimization for multi-modal chromatography, in: Neufeld, J.S., Buscher, U., Lasch, R., Möst, D., Schönberger, J. (Eds.), Operations Research Proceedings 2019, Springer International Publishing, Berlin, Heidelberg. (Accepted).

Cravero, I., Semplice, M., 2016. On the accuracy of WENO and CWENO reconstructions of third order on nonuniform meshes. J. Sci. Comput. 67, 1219–1246.

Danckwerts, P.V., 1953. Continuous flow systems: Distribution of residence times. Chem. Eng. Sci. 2, 1–13.

van Deemter, J.J., Zuiderweg, F.J., Klinkenberg, A., 1956. Longitudinal diffusion and resistance to mass transfer as causes of nonideality in chromatography. Chem. Eng. Sci. 5, 271–289.

Deitcher, R.W., Rome, J.E., Gildea, P.A., O'Connell, J.P., Fernandez, E.J., 2010. A new thermodynamic model describes the effects of ligand density and type, salt concentration and protein species in hydrophobic interaction chromatography. J. Chromatogr. A 1217, 199–208.

Diehl, M., Bock, H.G., Schlöder, J.P., Findeisen, R., Nagy, Z., Allgöwer, F., 2002. Real-time optimization and nonlinear model predictive control of processes governed by differential-algebraic equations. J. Process Control 12, 577–585.

Guiochon, G., 2002. Preparative liquid chromatography. J. Chromatogr. A 965, 129–161.

Guiochon, G., Felinger, A., Shirazi, D.G., Katti, A.M., 2006. Fundamentals of Preparative and Nonlinear Chromatography. Second ed., Elsevier/Academic Press, Amsterdam.

Hante, F.M., Sager, S., 2013. Relaxation methods for mixed-integer optimal control of partial differential equations. Comput. Optim. Appl. 55, 197–225.

Hesthaven, J.S., 2018. Numerical Methods for Conservation Laws: From Analysis to Algorithms. volume 18 of *Computational Science and Engineering Series*. Society for Industrial and Applied Mathematics (SIAM), Philadelphia (PA).

Hindmarsh, A.C., Brown, P.N., Grant, K.E., Lee, S.L., Serban, R., Shumaker, D.E., Woodward, C.S., 2005. SUNDIALS: Suite of nonlinear and differential/algebraic equation solvers. ACM Trans. Math. Software 31, 363–396.

Huuk, T.C., Hahn, T., Doninger, K., Griesbach, J., Hepbildikler, S., Hubbuch, J., 2017. Modeling of complex antibody elution behavior under high protein load densities in ion exchange chromatography using an asymmetric activity coefficient. Biotechnol. J. 12, 1600336.

Huuk, T.C., Hahn, T., Osberghaus, A., Hubbuch, J., 2014. Model-based integrated optimization and evaluation of a multi-step ion exchange chromatography. Sep. Purif. Technol. 136, 207–222.

Janson, J.C. (Ed.), 2011. Protein Purification: Principles, High Resolution Methods, and Applications. volume 54 of *Wiley Series in Methods of Biochemical Analysis*. Third ed., Wiley, Hoboken, NJ.

Jenkins, W.T., 1998. Three solutions of the protein solubility problem. Protein Sci. 7, 376–382.

Kallberg, K., Johansson, H.O., Bulow, L., 2012. Multimodal chromatography: An efficient tool in downstream processing of proteins. Biotechnol. J. 7, 1485–1495.

Karlsson, D., Jakobsson, N., Axelsson, A., Nilsson, B., 2004. Model-based optimization of a preparative ion-exchange step for antibody purification. J. Chromatogr. A 1055, 29–39.

Kirches, C., 2011. Fast Numerical Methods for Mixed-Integer Nonlinear Model-Predictive Control. Vieweg+Teubner Verlag, Wiesbaden.

Kirches, C., Lenders, F., Manns, P., 2020. Approximation properties and tight bounds for constrained mixed-integer optimal control. SIAM J. Control Optim. 58, 1371–1402.

Leineweber, D.B., Bauer, I., Schäfer, A., Bock, H.G., Schlöder, J.P., 2003. An efficient multiple shooting based reduced SQP strategy for large-scale dynamic process optimization (parts I and II). Comput. Chem. Eng. 27, 157–174.

Leweke, S., von Lieres, E., 2018. Chromatography analysis and design toolkit (CADET). Comput. Chem. Eng. 113, 274–294.

von Lieres, E., Andersson, J., 2010. A fast and accurate solver for the general rate model of column liquid chromatography. Comput. Chem. Eng. 34, 1180–1191.

Manns, P., Kirches, C., 2018. Multi-dimensional sum-up rounding for elliptic control systems. DFG SPP 1962 Preprint URL: `https://spp1962.wias-berlin.de/preprints/080.pdf`. (Submitted to SIAM Journal on Numerical Analysis).

Manns, P., Kirches, C., 2020. Improved regularity assumptions for partial outer convexification of mixed-integer PDE-constrained optimization problems. ESAIM Control Optim. Calc. Var. 26, 32.

Melander, W.R., Horváth, C., 1977. Salt effects on hydrophobic interactions in precipitation and chromatography of proteins: An interpretation of the lyotropic series. Arch. Biochem. Biophys. 183, 200–215.

Mollerup, J.M., 2006. Applied thermodynamics: A new frontier for biotechnology. Fluid Phase Equilib. 241, 205–215.

Mollerup, J.M., 2007. The thermodynamic principles of ligand binding in chromatography and biology. J. Biotechnol. 132, 187–195.

Mollerup, J.M., 2008. A review of the thermodynamics of protein association to ligands, protein adsorption, and adsorption isotherms. Chem. Eng. Technol. 31, 864–874.

Nfor, B.K., Noverraz, M., Chilamkurthi, S., Verhaert, P.D.E.M., van der Wielen, L.A., Ottens, M., 2010. High-throughput isotherm determination and thermodynamic modeling of protein adsorption on mixed mode adsorbents. J. Chromatogr. A 1217, 6829–6850.

Nfor, B.K., Zuluaga, D.S., Verheijen, P.J.T., Verhaert, P.D.E.M., van der Wielen, L.A.M., Ottens, M., 2011. Model-based rational strategy for chromatographic resin selection. Biotechnol. Progr. 27, 1629–1643.

Nocedal, J., Wright, S.J., 2006. Numerical Optimization. Second ed., Springer Verlag, Berlin Heidelberg New York.

Osberghaus, A., Hepbildikler, S., Nath, S., Haindl, M., von Lieres, E., Hubbuch, J., 2012a. Determination of parameters for the steric mass action model—A comparison between two approaches. J. Chromatogr. A 1233, 54–65.

Osberghaus, A., Hepbildikler, S., Nath, S., Haindl, M., von Lieres, E., Hubbuch, J., 2012b. Optimizing a chromatographic three component separation: A comparison of mechanistic and empiric modeling approaches. J. Chromatogr. A 1237, 86–95.

Persson, P., Gustavsson, P.E., Zacchi, G., Nilsson, B., 2006. Aspects of estimating parameter dependencies in a detailed chromatography model based on frontal experiments. Process Biochem. 41, 1812–1821.

Potschka, A., 2014. A Direct Method for Parabolic PDE Constrained Optimization Problems. volume 9 of *Advances in Numerical Mathematics*. Springer Fachmedien Wiesbaden, Wiesbaden.

Rathore, A.S., Kumar, D., Kateja, N., 2018. Recent developments in chromatographic purification of biopharmaceuticals. Biotechnol. Lett. 40, 895–905.

Sager, S., 2005. Numerical methods for mixed-integer optimal control problems. Der andere Verlag, Tönning, Lübeck, Marburg.

Sager, S., Bock, H.G., Diehl, M., 2012. The integer approximation error in mixed-integer optimal control. Math. Progam. 133, 1–23.

Sager, S., Jung, M., Kirches, C., 2011. Combinatorial integral approximation. Math. Methods Oper. Res. 73, 363–380.

Schiesser, W.E., 1991. The Numerical Method of Lines. Academic Press, San Diego, CA.

Schmidt-Traub, H., Schulte, M., Seidel-Morgenstern, A. (Eds.), 2012. Preparative Chromatography. Second ed., Wiley–VCH, Weinheim.

Shu, C.W., 1998. Essentially non-oscillatory and weighted essentially non-oscillatory schemes for hyperbolic conservation laws, in: Quarteroni, A. (Ed.), Advanced Numerical Approximation of Nonlinear Hyperbolic Equations: Lectures given at the 2nd Session of the Centro Internazionale Matematico Estivo (C.I.M.E.) held in Cetraro, Italy, June 23–28, 1997. Springer Berlin Heidelberg, Berlin, Heidelberg, pp. 325–432.

Shu, C.W., 2009. High order weighted essentially nonoscillatory schemes for convection dominated problems. SIAM Rev. 51, 82–126.

Staby, A., Rathore, A.S., Ahuja, S. (Eds.), 2017. Preparative Chromatography for Separation of Proteins. Wiley Series in Biotechnology and Bioengineering, John Wiley & Sons, Hoboken, NJ.

U.S. Food and Drug Administration, 2004. Guidance for industry: PAT—A framework for innovative pharmaceutical development, manufacturing, and quality assurance. URL: `https://www.fda.gov/media/71012/download`.

Wächter, A., Biegler, L.T., 2006. On the implementation of an interior-point filter line-search algorithm for large-scale nonlinear programming. Math. Progam. 106, 25–57.

Wang, G., Hahn, T., Hubbuch, J., 2016. Water on hydrophobic surfaces: Mechanistic modeling of hydrophobic interaction chromatography. J. Chromatogr. A 1465, 71–78.

Wang, R., Feng, H., Spiteri, R.J., 2008. Observations on the fifth-order WENO method with non-uniform meshes. Appl. Math. Comput. 196, 433–447.

Wolfe, L.S., Barringer, C.P., Mostafa, S.S., Shukla, A.A., 2014. Multimodal chromatography: Characterization of protein binding and selectivity enhancement through mobile phase modulators. J. Chromatogr. A 1340, 151–156.

Zhang, K., Liu, X., 2016. Mixed-mode chromatography in pharmaceutical and biopharmaceutical applications. J. Pharm. Biomed. Anal. 128, 73–88.

Zhao, G., Dong, X.Y., Sun, Y., 2009. Ligands for mixed-mode protein chromatography: Principles, characteristics and design. J. Biotechnol. 144, 3–11.

Zhu, M., Carta, G., 2016. Protein adsorption equilibrium and kinetics in multimodal cation exchange resins. Adsorption 22, 165–179.